Hotspot Cooling Performance of a Submerged Water Jet via Infrared Thermometry

Tanvir Ahmed Chowdhury, Chance Brewer, and Shawn A. Putnam
Department of Mechanical and Aerospace Engineering
University of Central Florida, Orlando, FL 32816
chowdhurytanvir@knights.ucf.edu, chanceb@knights.ucf.edu, shawn.putnam@ucf.edu

ABSTRACT

Liquid jet impingement is one of the most effective methods for dissipating local hotpot heat fluxes in microelectronics. Due to its normal incident flow-field, jet impingement cooling can achieve heat transfer coefficients (HTCs) approaching $\approx$1 MW/m^2·K due to its ability to thin the local thermal boundary layer in the stagnation region. This experimental study presents HTC data for water jet impingement cooling of a laser heated Hafnium (Hf) thin-film on glass. A laser diode induces local hotspots for either a steady- or pulsed-laser operation mode. The hotspots have areas ranging within 0.04 mm^2 to 0.2 mm^2 and heat fluxes up to $\approx$3.5 MW/m^2. A submerged jet impingement configuration is pursued with an inlet jet diameter of $\sim$1.2 mm, jet nozzle to hotspot/surface distance of $\sim$3.2 mm, and the jet Reynolds Number of $\sim$2004. The HTCs are measured using infrared (IR) thermometry using a 1.5-5 μm spectral resolution FLIR camera. Also investigated is the spatial dependence of the HTC relative to the offset between jet/wall stagnation point and the center of the local hotspot. For example, for impinging jets that are co-aligned with the hotspot center, HTCs of $\sim$650 kW/m^2·K and $\sim$470 kW/m^2·K are measured for steady and pulsed-modulated laser heating (respectively), whereas, for offsets beyond $\sim$6 mm (x/D >5), the measured HTCs are <100 kW/m^2·K.

KEY WORDS: Hotspot Cooling, IR Thermography, Submerged Jet Impingement

NOMENCLATURE

A	Area, mm^2
x	Distance between jet center & hotspot, mm
D	Diameter of the jet nozzle, mm
Re	Reynolds number
H	Jet nozzle to heated surface distance, mm
f	Frequency, Hz
HTC, h	Heat Transfer Coefficient, kW/m^2-K
k	Thermal conductivity, W/m-K
C_p	Volumetric heat capacity, J/K-m^3
t	Time, s
Hf	Hafnium
Q	Heating rate, W
T	Temperature, K
q	Heat flux, MW/m^2
R	Reflectance
Nu	Nusselt number

Greek symbols

δ	Thermal penetration depth, nm
δ_{th}	Thermal boundary layer thickness, nm

Subscripts

eqv	Equivalent
HS	Hotspot
water	Water
mod	Modulation
jet	Jet

INTRODUCTION

Active cooling is a thermal management process where an external device is used to enhance the cooling performance (ideally, in real-time using sensor feedback and controls). Jet impingement is an attractive thermal management technique - especially for mitigating extreme heat fluxes from local hotspots [1]–[16]. For example, according to an estimation by Mitsuake et al. [16], future technologies will demand active cooling methods that can mitigate heat fluxes of the order of 100 MW/m^2. Submerged jet impingement is one of the most promising methods to achieve such a goal. Coupled to this goal, a detailed understanding of the heat transfer coefficient (HTC) is arguably the most important metric for improving the cooling performance. In result, over the last several decades, research on predicting the HTC for various experimental conditions has been of utmost importance [17]–[19]. One of the key parameters for submerged jet impingement is the mean jet velocity (or jet Reynolds number). An increase in jet impingement velocity (or Reynolds number) results in an increase in the HTC, where the highest HTCs are observed within the stagnation zone (or at the edge of stagnation zone) [1]. Another key important parameter is the separation distance between the jet nozzle outlet and the heated wall surface H (or the ratio of H/D, where D is the outlet diameter of the submerged jet). It has been found that maximum HTCs are achieved when $H/D < 6$ [1]. This is potentially due to that the potential core of the jet coincides with the size of stagnation zone. For H/D <6, we are unaware of published work that provides analytic solution of the flow-field for a submerged jet, which is a key motivator for the experimental studies discussed herein. Moreover, while there has been many investigations on jet impingement cooling, in most cases the studied heating condition is that of a uniformly heated surface. This is contrary to the optimal potential for jet impingement cooling, which is for mitigating extreme hotspot heat fluxes.

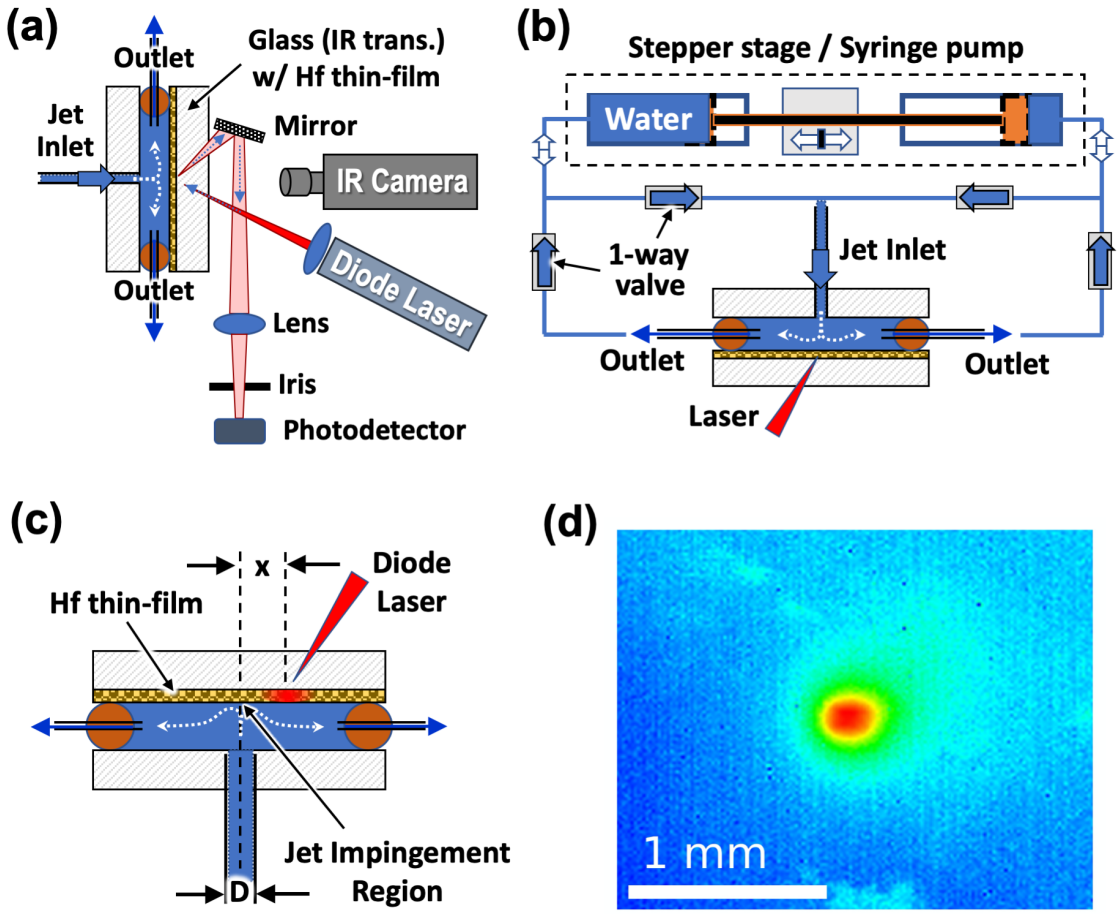

Figure. 1: Overview of the submerged jet impingement setup for cooling local hotspots generated by a focused diode laser. (a) Laser heating schematic emphasizing the in-situ IR thermometry method and laser power monitoring with a photodetector. (b) Schematic of the jet impingement flow-loop using a dual syringe pump configuration and multiple 1-way flow valves. (c) Schematic illustration of the fluid-cell for submerged jet impingement with an offset (x) between jet impingement axis and the hotspot center. The hotspot is generated by laser heating the Hf thin-film (thickness: ≈100 nm) on an IR transparent glass window. (d) IR image corresponding to laser heating the Hf/glass substrate with stagnant water in the fluid-cell - e.g., no jet flow (Re $\approx$ 0) and $q \approx$ 1.4 MW/m^2.

This study investigates the cooling performance (HTC) of submerged water jet impingement in a hotspot heating configuration. The key aspects investigated are (1) the role of the heating frequency on the overall HTC and (2) the impact of the offset between jet stagnation point and the hotspot center on the HTC. In regards to the latter, HTC data is provided in terms of the x/D ratio, where x is the offset distance between the jet and hot-spot center, and D is the diameter of the jet nozzle.

EXPERIMENTAL SETUP

Figure 1 illustrates the experimental setup used in this study. Fig. 1a depicts how a diode laser is used to heat a Hafnium (Hf) thin-film on an IR transparent glass window/substrate. This Hf/glass sample was made by depositing 100 nm of Hf on V-coated glass substrate via DC magnetron sputtering. As illustrated in Figs. 1a-c, a submerged jet/coolant chamber is created using an O-ring seal between the Hf thin-film and another glass window. Jet input was directed through the center of glass window, so that jet can impinge co-aligned with the Hf surface normal. The coolant chamber has two jet/water outlets via two syringe needles passing through the O-ring seal. The diode laser source is of blue laser light (450 nm) and is partially absorbed by the Hf thin-film (transmission $<$ 0.1%, reflection $<$ 45%). A function generator is used to control the modulation frequency of the diode laser heating source. In this study, two different types of heating condition were used: namely, 'steady' laser heating with a constant laser output power of ∼350 mW or 'pulsed' laser heating with an average laser output power of ∼350 mW. For example, for the pulsed heating condition, the laser power is a square-wave with a peak power of ∼700 mW modulated at frequencies of either f_{mod} ≈3, 20, or 75 Hz (duty cycle of 50%, for all pulsed heating conditions). As shown in Fig. 1a, a focusing lens is

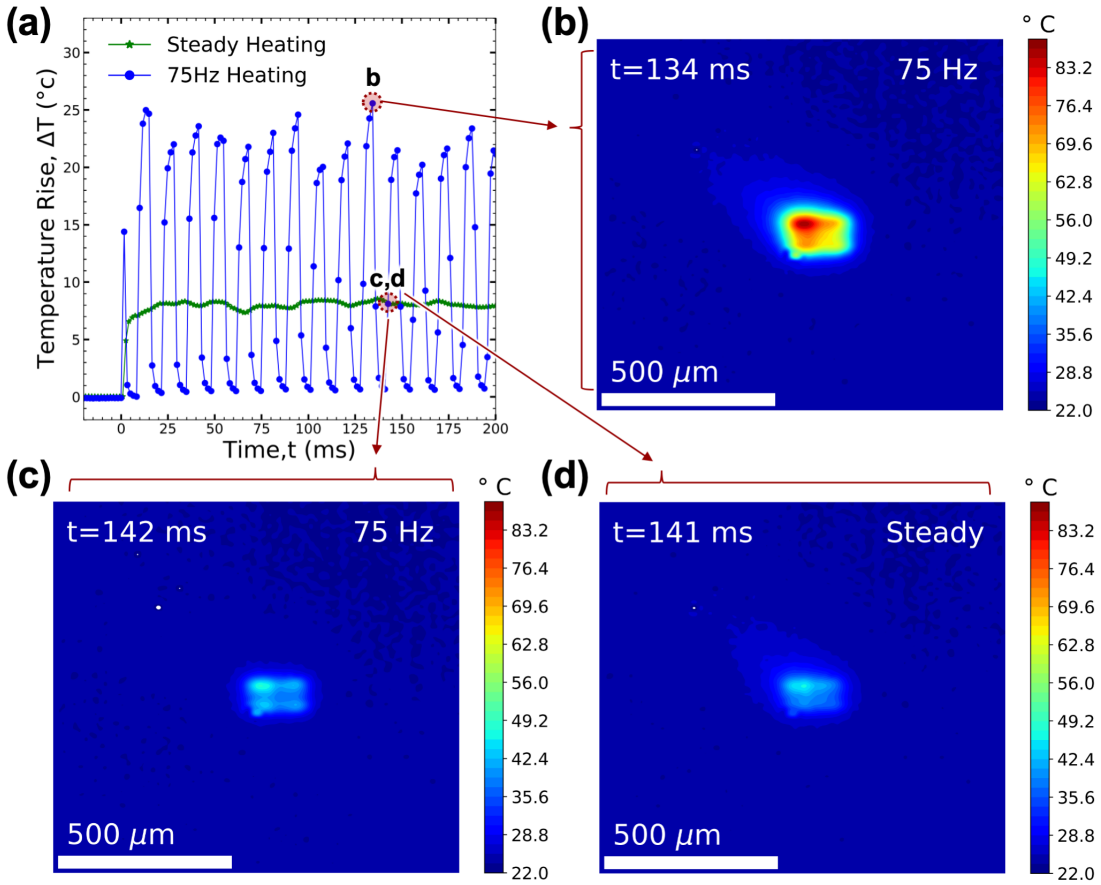

Figure. 2: Spatiotemporal evolution of the hotspot surface temperature. (a) Temporal plots of the area-averaged hotspot temperature rise ($\Delta T = T_{HS} - T_{jet}$) for both steady- and modulated-heating. The incident water/jet corresponds to a jet Reynolds number of Re $\approx$ 2004 at an inlet temperature of 23.5$\pm$0.5 °C. (b) is the corresponding IR camera data of the hotspot temperature distribution for a peak in the modulated heating cycle. (c) and (d) are the corresponding hotspot temperature distributions for both modulated- and steady-heating (respectively) at $t \approx 140$ ms, where $t < 0$ms corresponds to laser heat source in the 'off' state.

used to control the area/size of local hotspot generated in Hf thin-film after laser transmission through the glass substrate. The laser power can be adjusted to control the hotspot heat flux. For this study, the maximum (average) hotspot heat flux was 3.5 MW/m^2 (for both steady- and modulated-heating settings) at the Hf/jet interface (i.e., the interface between the submerged water jet and Hf thin-film hotspot created by the 450 nm diode laser). We note that roughly 44% of the diode laser light was reflected from the Hf/glass heater sample. As shown in Fig. 1a, the remaining (reflected) laser light is monitored by a photodetector. The response of the photodetector provides in-situ monitoring of temporal heat input, which is independent of spatiotemporal infrared (IR) camera measurements.

A FLIR IR camera is used to capture the spatiotemporal evolution of temperature profile of the Hf thin-film (spectral sensitivity: 1.5-5 μm, frame rate: 603 frames-per-second (fps), window size: 160 $\times$ 128 pixels, pixel size: $\sim$15.1 μm). The data for each experiment was taken for $\sim$60 seconds. The IR camera was calibrated using a K-type thermocouple and the procedure outlined by the FLIR for estimating the emissivity of the Hf thin-film and the transmissivity of glass window/substrate [20]. The effective heating radius of laser beam (and/or hotspot) was $\sim$126 μm and the thickness of Hf thin-film was $\sim$100 nm. For this beam size over the $\sim$100 nm thick Hf thin-film the thickness dependent temperature decay is $\sim$0% [21]. Hence it can be assumed that both sides of Hf thin film have the same temperature.

Figure 1b depicts the flow-loop setup based on a dual syringe pump configuration. Two stainless steel piston syringes are connected through a computer-controlled stepper stage. If the stepper/translation stage is displaced in one direction, then the water coolant is simultaneously displaced 'out-of' one piston/syringe and 'in-to' the other piston/syringe. The set of four one-way valves allow a forward jet operation regardless of the pumping direction (or displacement direction of the stepper/translation stage).

Figure 1c depicts the 'offset' between stagnation point of the jet and the center of the hotspot. The distance between the hotspot center and stagnation point is defined as x. We

normalize this offset by the diameter of the jet nozzle - e.g., x/D, where D is the diameter of the jet nozzle. The distance between the jet nozzle outlet and the Hf surface is $H \approx 3.175$ mm, which corresponds to $H/D \approx 2.64$.

Figure 1d is an example of the hotspot created by the diode laser heating the Hf thin-film with a stagnant water pool in the fluid chamber (i.e., for no jet impingement, Re = 0). The red-spot (or red-ellipse) in this IR camera image is the hotspot. In our temperature data/image analysis, the hotspot area was segmented to monitor the spatiotemporal evolution with a comparative understanding of the jet cooling performance for different experimental conditions. For example, first, the hotspot was focused on the hafnium surface with stagnant water in the coolant fluid-cell (i.e., hotspot cooling by natural convection only). Then, the canny edge detection method [22] was used to segment the hotspot region-of-interest (ROI). Then, this segmented hotspot ROI was used as a mask for all subsequent IR image/data analysis, allowing us to keep track of the temperature of the hotspot ROI area while cooling with a submerged water jet (Re$\sim$2004). Then, the spatiotemporal IR temperature recordings over the hotspot area were converted to an area-averaged hotspot temperature.

RESULTS & DISCUSSION

Figure 2a displays the temporal evolution of the hotspot 'area-averaged' temperature for both steady heating and modulated heating at 75 Hz at zero offset $x/D = 0$ from $t = 0$ seconds (i.e., incident heating with a steady jet (Re = 2004)) to time $t = 200$ ms. The temperature rise corresponds to difference between the area-averaged hotspot temperature (T_{HS}) and the temperature of the incident water jet (T_{jet}). The highlighted/indicated peak point 'b' at $t = 134$ ms in Fig. 2a corresponds to a peak temperature rise for modulated heating at $f_{mod} = 75$ Hz (Fig. 2b provides a snapshot image of the IR thermal map acquired at $t = 134$ ms). Whereas, the highlighted points 'c,d' in Fig. 2a correspond to hotspot temperatures for both modulated laser heating (75 Hz) and steady laser heating at times $t = 142$ ms and $t = 141$ ms, respectively. Figs. 2c and 2d are snapshot images of the IR thermal map acquired at $t = 142$ ms (modulated heating - 75 Hz) and $t = 141$ ms (steady heating), respectively.

The temperature distribution shown in Fig. 2b (point 'b' in Fig. 2a) shows how the impinging jet influences the hotspot temperature, where heat is carried away from the hotspot center by the jet's anisotropic flow-field. This characteristic is further exemplified with comparison to the hotspot temperature distribution for a stagnant fluid (see, Fig. 1d relative to Fig. 2b). As depicted in Fig. 2d, a similar anisotropic flow-field and heat transport characteristic is observed for the steady jet impingement cooling configuration. Whereas, in Fig. 2c, the temperature distribution is less anisotropic. We note that the provided temperature distribution in Fig. 2c represents laser heating near the start of the 'On' period of the pulse modulation (point, 'c' in Fig. 2a). These results also indicate that at the early stages of pulsed-heating process, the impinging jet is not significantly dissipating heat to the nearby water (or Hf thin-film surface) by forced convection. For example, comparison between the temperature distributions in Figs. 2c and 2d show that for the same corresponding temperature rise ($\Delta T \approx 8.2$ K), the steady-heating configuration provides much more convective heat transfer than that for modulated-heating at $\sim$75 Hz. This observation is emphasized further by our increased HTC results for steady-heating relative to modulated-heating with the same spatiotemporally-averaged hotspot heat fluxes.

As stated previously, for comparison between these different heating conditions, this study segments the hotspot ROI relative to that of the stagnant water condition to generate a consistent ROI mask for later calculation of the area-averaged hotspot temperature. This process also helps resolve the other data analysis bottleneck associated with how to systematically distinguish between the modulated- and steady-heating conditions. As shown in Fig. 2, the modulated-heating configuration induces both spatially and temporally anisotropic flow-fields throughout the jet cooling process due to the 'on/off' nature of the heating source. On the other hand, for the steady-heating configuration, after a few milliseconds only a 'spatially' anisotropic flow-field is observed. Because of these observations, this study analyzes the area-averaged hotspot temperature data (based on a stagnant water hotspot mask) over many frames ($\approx$ 603) or long times relative to the heating period for our pulse-modulated heat source (e.g, ($t \approx 1$ s $>> 1/f$)). Such analysis, allows the modulated temperature rise (ΔT) profiles (blue lines/data in Fig. 2a) to appear analogous to the steady temperature rise profile (green lines/data in Fig. 2a). Then, the time- and spatially-averaged hotspot temperature data within $t = 40$ and 50 seconds can be relatively compared in terms of an overall HTC - respective to the different steady- or modulated-heating conditions. In this regard, we define a spatiotemporally-averaged hotspot temperature as T_{eqv}. Then, a spatiotemporally-averaged HTC can be calculated via applying Newtons' law of cooling:

$$HTC = \frac{q}{\Delta T_{eqv}}, \tag{1}$$

where q is the hotspot heat flux and $\Delta T_{eqv} = T_{eqv} - T_{jet}$ is the temperature difference between impinging water jet (T_{jet}) and hotspot (T_{eqv}). Based on the experimental configuration, the wall heat flux follows as

$$q = \frac{Q(1-R)}{A_{HS}}, \tag{2}$$

where Q is the average power of the laser diode, R is the reflectance of the Hf/glass surface and A_{HS} is the area of the hotspot mask. The corresponding dimensionless HTC or Nusselt number (Nu) is defined as

$$Nu = \frac{HTC \times D}{k_{water}}, \tag{3}$$

where D is the jet diameter and k_{water} is the thermal conductivity of water/jet.

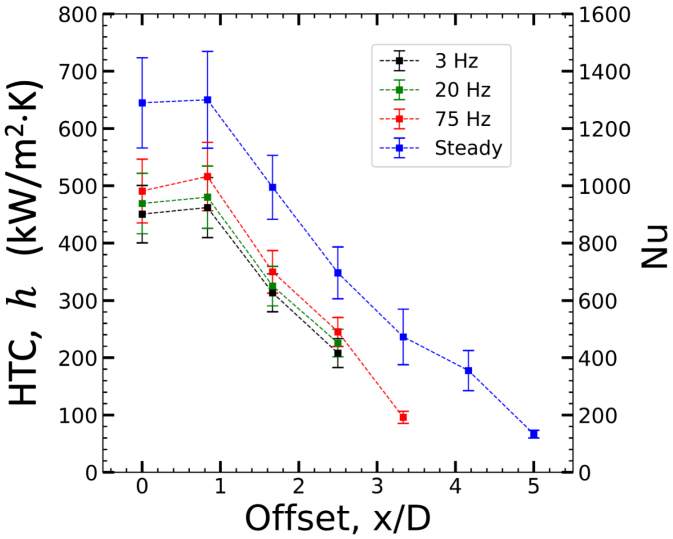

Figure. 3: Heat transfer coefficients measured as a function of the offset ratio and heating condition. For both steady and modulated heating ($f_{mod} \approx$ 3, 20, and 75 Hz), the average incident laser power was 350 mW, generating a spatiotemporally-averaged hotspot heat flux of 3.5 MW/m^2 heat flux.

Figure 3 presents the measured HTC (left axis) and Nu# (right axis) results from this study within a 95% confidence interval. Uncertainty in laser power measurements, reflectivity of Hf surface, hotspot area, heated surface temperature, and inlet water/jet temperature were considered while calculating this 95% confidence interval. For an offset ratio within of $0 \leq x/D \leq$0.83, the HTCs measured for steady- and modulated-heating (f_{mod} = 75 Hz) are $\approx$ 650 kW/m^2·K and $\approx$ 495 kW/m^2·K, respectively. As shown in Fig. 3, the HTC peaks around the edge of the jet impingement zone (i.e., maximum HTCs are observed for $x/D \approx 0.83$. This corresponds to the jet-impingement region where the flow-field acceleration is at a maximum [23], [24]. Also, as shown in Fig. 3 for $x > D$, the HTC steadily decreases with increases in the offset between the jet stagnation point and the hotspot center. As expected, away from the jet impingement region, the impact of jet's potential core diminishes; and, hence, the HTC decreases. Also, away from jet impingement region, the thickness of the hydraulic boundary layer starts to grow, which also contributes to decreases in the HTC.

Another interesting result from this investigation is that the HTC is less for modulated heating (relative to that for steady heating). This HTC result in Figure 3 is also represented in the IR temperature maps/images in Figs. 2c and 2d for $x/D \approx 0$. As shown, more flow-field convection is observed for steady-heating (Fig. 2d) compared to that for modulated-heating (Fig. 2c) - even though an equivalent hotspot temperature is observed for both cases at $t = 140$ ms - see the corresponding

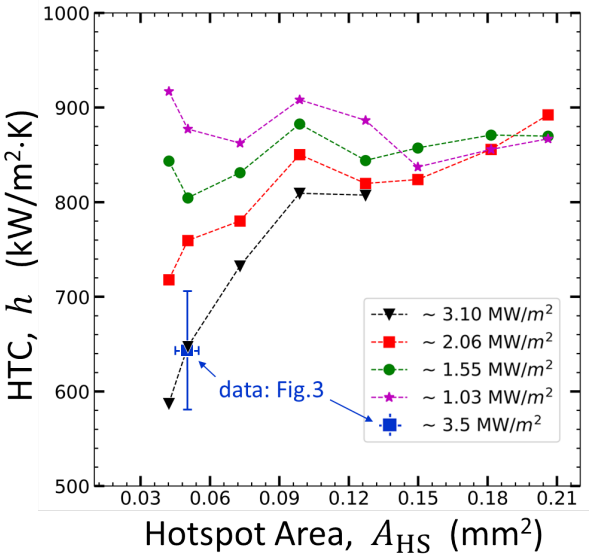

Figure. 4: Heat transfer coefficients measured as a function of hotspot area. The data sets correspond to measurements for steady heating at different hotspot heat fluxes.

'c,d' points in Fig. 2a. We note that the steady heating case can be considered as modulated-heating at $f_{mod} \approx \infty$ Hz. From this study, it can be inferred that the HTC is inversely proportional to the heating-frequency (while keeping the same average hotspot heating power). The thermal penetration depth is also inversely proportional to the heating-frequency [25] - e.g., the thermal penetration depth follows as,

$$\delta = \sqrt{\frac{k}{\pi f_{mod} C_p}}, \tag{4}$$

where f_{mod} is the modulation frequency of the heating source and C_p and k are the volumetric heat capacity and the thermal conductivity of the fluid coolant/jet. Given that the thermal penetration (δ) scales proportionally with the thickness of the thermal boundary layer (δ_{th}), the HTC is expected to scale inversely with the thermal penetration depth (or directly with the heating frequency) - i.e.,

$$HTC \propto \frac{k}{\delta} \propto \sqrt{f_{mod} k C_p}. \tag{5}$$

Another important finding from this study is that rather significant HTCs are observed even for hotspot offset ratios within $2 < x/D < 3$ (e.g., $h >$ 100kW/m^2·K, where $h|_{\frac{x}{D}\sim 3} \approx \frac{1}{3} h|_{\frac{x}{D}<1}$). These HTCs are still rather high compared to that from other cooling methods [26]. Thus, this result supports the potential for a single jet to efficiently cool a distribution of different potential hotspot locations (as long as $x/D < 5$) or that precise jet alignment with a hotspot is not a critical design metric.

Figure 4 provides HTC data for the effects of the size of the hotspot on the cooling efficiency. The blue square data point represents the HTC measured for steady heating ($q \approx 3.5\text{MW/m}^2$) in Figure 3 at $x/D \approx 0$. Error bars for the other data in Figure 4 are indicative of that of the blue-square data. As shown, the HTC decreases with decreases in hot-spot area (especially for higher hotspot heat fluxes). Additional studies as a function of offset are required for further interpretation.

CONCLUSION

This study investigated the HTC for submerged jets cooling local hotspots as a function of jet offset, heating frequency, wall heat flux, and the area of the local hotspot. It was found that the highest HTC can be expected with steady heating conditions and for cooling within the stagnation zone (e.g., offset ratios within $x/D < 1$). Even with offsets beyond $x \approx 3D$, jet impingement cooling was highly efficient providing HTCs beyond 100 kW/m^2·K.

Acknowledgments

This material is based on research sponsored by the U.S. Israel Binational Science Foundation under Grant No. 2016399. The views and conclusions contained herein are those of the authors and should not be interpreted as necessarily representing the official policies or endorsements, either expressed or implied, of the Office of the US Israel Binational Science Foundation. The authors thank the incredibly helpful feedback from Gennady Ziskind and Tomer Shockner. The authors also thank Khan Mohammad Rabbi for helpful technical discussions in lab. The authors are grateful for NumPy [27], SciPy [28], Pandas [29], Matplotlib [30] packages that helped immensely during the data analysis.

References

[1] N. Zuckerman and N. Lior, "Jet impingement heat transfer: Physics, correlations, and numerical modeling," ser. Advances in Heat Transfer, G. A. Greene, J. P. Hartnett†, A. Bar-Cohen, and Y. I. Cho, Eds. Elsevier, 2006, vol. 39, pp. 565 – 631.

[2] S. Ndao, Y. Peles, and M. K. Jensen, "Experimental investigation of flow boiling heat transfer of jet impingement on smooth and micro structured surfaces," *International Journal of Heat and Mass Transfer*, vol. 55, no. 19, pp. 5093 – 5101, 2012. [Online]. Available: http://www.sciencedirect.com/science/article/pii/S0017931012003225

[3] C.-F. Ma and A. Bergles, "Jet impingement nucleate boiling," *International Journal of Heat and Mass Transfer*, vol. 29, no. 8, pp. 1095 – 1101, 1986. [Online]. Available: http://www.sciencedirect.com/science/article/pii/0017931086901407

[4] D. Zhou, C. Ma, and J. Yu, "Boiling hysteresis of impinging circular submerged jets with highly wetting liquids," *International Journal of Heat and Fluid Flow*, vol. 25, no. 1, pp. 81–90, feb 2004. [Online]. Available: https://linkinghub.elsevier.com/retrieve/pii/S0142727X03001280

[5] S. N. Joshi and E. M. Dede, "Effect of sub-cooling on performance of a multi-jet two phase cooler with multi-scale porous surfaces," *International Journal of Thermal Sciences*, vol. 87, pp. 110 – 120, 2015. [Online]. Available: http://www.sciencedirect.com/science/article/pii/S1290072914002403

[6] M. J. Rau, E. M. Dede, and S. V. Garimella, "Local single- and two-phase heat transfer from an impinging cross-shaped jet," *International Journal of Heat and Mass Transfer*, vol. 79, pp. 432 – 436, 2014. [Online]. Available: http://www.sciencedirect.com/science/article/pii/S0017931014006991

[7] L. Qiu, S. Dubey, F. H. Choo, and F. Duan, "Recent developments of jet impingement nucleate boiling," *International Journal of Heat and Mass Transfer*, vol. 89, pp. 42–58, 2015. [Online]. Available: http://dx.doi.org/10.1016/j.ijheatmasstransfer.2015.05.025

[8] P. Valiorgue, T. Persoons, A. McGuinn, and D. Murray, "Heat transfer mechanisms in an impinging synthetic jet for a small jet-to-surface spacing," *Experimental Thermal and Fluid Science*, vol. 33, no. 4, pp. 597 – 603, 2009. [Online]. Available: http://www.sciencedirect.com/science/article/pii/S0894177708001763

[9] D. B. M. M. F. Colin Glynn, Tadhg O'Donovan, "Jet impingement cooling," *Proceedings of the 9th UK National Heat Transfer Conference*, pp. 5–6, 2005.

[10] Y. hao Qiu and Z. hua Liu, "Critical heat flux of steady boiling for saturated liquids jet impinging on the stagnation zone," *International Journal of Heat and Mass Transfer*, vol. 48, no. 21, pp. 4590 – 4597, 2005. [Online]. Available: http://www.sciencedirect.com/science/article/pii/S0017931005004023

[11] S.-M. Lin, H.-F. Liu, W.-R. Wang, S. Y. Lee, C.-Y. Cheng, and C.-Y. Li, "Optimum design and heat transfer correlation equation of a mini radiator with jet impingement cooling," *Applied Thermal Engineering*, vol. 89, pp. 727 – 737, 2015. [Online]. Available: http://www.sciencedirect.com/science/article/pii/S1359431115006249

[12] C.-B. Kim, C. Leng, X.-D. Wang, T.-H. Wang, and W.-M. Yan, "Effects of slot-jet length on the cooling performance of hybrid microchannel/slot-jet module," *International Journal of Heat and Mass Transfer*, vol. 89, pp. 838 – 845, 2015. [Online]. Available: http://www.sciencedirect.com/science/article/pii/S0017931015006122

[13] Z. Zhao, Y. Peles, and M. K. Jensen, "Microjet impingement boiling on a structured-porous surface," *ASME 2012 Third International Conference on Micro/Nanoscale Heat and Mass Transfer*, pp. 411–417, 2013.

[14] X. Liu, L. A. Gabour, and V. Lienhard, J. H., "Stagnation-Point Heat Transfer During Impingement of Laminar Liquid Jets: Analysis Including Surface Tension," *Journal of Heat Transfer*, vol. 115, no. 1, pp. 99–105, 02 1993. [Online]. Available: https://doi.org/10.1115/1.2910677

[15] Y.-J. Chen, Y.-Y. Li, and Z.-H. Liu, "Experimental study on the stagnation line heat transfer characteristics with high-velocity free slot jet impingement boiling," *International Journal of Heat and Mass Transfer*, vol. 91, pp. 282 – 292, 2015. [Online]. Available: http://www.sciencedirect.com/science/article/pii/S0017931015008327

[16] Y. Mitsutake and M. Monde, "Ultra High Critical Heat Flux During Forced Flow Boiling Heat Transfer With an Impinging Jet ," *Journal of Heat Transfer*, vol. 125, no. 6, pp. 1038–1045, 11 2003. [Online]. Available: https://doi.org/10.1115/1.1621899

[17] T. Park, H. Choi, J. Yoo, and S. Kim, "Streamline upwind numerical simulation of two-dimensional confined impinging slot jets," *International Journal of Heat and Mass Transfer*, vol. 46, no. 2, pp. 251 – 262, 2003.

[18] J. W. Baughn, A. E. Hechanova, and X. Yan, "An Experimental Study of Entrainment Effects on the Heat Transfer From a Flat Surface to a Heated Circular Impinging Jet," *Journal of Heat Transfer*, vol. 113, no. 4, pp. 1023–1025, 11 1991. [Online]. Available: https://doi.org/10.1115/1.2911197

[19] T. Germain, T. A. Chowdhury, J. Carter, and S. A. Putnam, "Measuring heat transfer coefficients for microchannel jet impingement using time-domain thermoreflectance," in *2018 17th IEEE Intersociety Conference on Thermal and Thermomechanical Phenomena in Electronic Systems (ITherm)*, May 2018, pp. 449–454.

[20] R. Danjoux, "Window and external optics transmittance," http://support.flir.com/Answers/A817T/A817-T560472_A-en-US%20Technical%20publication%2060%20Window%20or%20External%20Optics%20Transmittance.pdf, accessed: 2020-03-04.

[21] J. L. Braun and P. E. Hopkins, "Upper limit to the thermal penetration depth during modulated heating of multilayer thin films with pulsed and continuous wave lasers: A numerical study," *Journal of Applied Physics*, vol. 121, no. 17, p. 175107, may 2017. [Online]. Available: http://aip.scitation.org/doi/10.1063/1.4982915

[22] J. Canny, "A computational approach to edge detection," *IEEE Transactions on Pattern Analysis and Machine Intelligence*, vol. PAMI-8, no. 6, pp. 679–698, Nov 1986.

[23] J. H. Lienhard, "Heat Transfer by Impingement of Circular Free-Surface Liquid Jets," *Invited Keynote Paper, 18th National and 7th ISHMT-ASME Heat and Mass Transfer Conference*, January 2006.

[24] B. Webb and C.-F. Ma, "Single-phase liquid jet impingement heat transfer," ser. Advances in Heat Transfer, J. P. Hartnett and T. F. Irvine, Eds. Elsevier, 1995, vol. 26, pp. 105 – 217. [Online]. Available: http://www.sciencedirect.com/science/article/pii/S006527170870296X

[25] Y. K. Koh and D. G. Cahill, "Frequency dependence of the thermal conductivity of semiconductor alloys," *Phys. Rev. B*, vol. 76, p. 075207, Aug 2007. [Online]. Available: https://link.aps.org/doi/10.1103/PhysRevB.76.075207

[26] M. Mehrvand and S. A. Putnam, "Probing the Local Heat Transfer Coefficient of Water-Cooled Microchannels Using Time-Domain Thermoreflectance," *Journal of Heat Transfer*, vol. 139, no. 11, 06 2017, 112403. [Online]. Available: https://doi.org/10.1115/1.4036691

[27] T. Oliphant, "NumPy: A guide to NumPy," USA: Trelgol Publishing, 2006–, [Online; accessed ¡today¿]. [Online]. Available: http://www.numpy.org/

[28] P. Virtanen, R. Gommers, T. E. Oliphant, M. Haberland, T. Reddy, D. Cournapeau, E. Burovski, P. Peterson, W. Weckesser, J. Bright, S. J. van der Walt, M. Brett, J. Wilson, K. Jarrod Millman, N. Mayorov, A. R. J. Nelson, E. Jones, R. Kern, E. Larson, C. Carey, İ. Polat, Y. Feng, E. W. Moore, J. Vand erPlas, D. Laxalde, J. Perktold, R. Cimrman, I. Henriksen, E. A. Quintero, C. R. Harris, A. M. Archibald, A. H. Ribeiro, F. Pedregosa, P. van Mulbregt, and S. . . Contributors, "SciPy 1.0: Fundamental Algorithms for Scientific Computing in Python," *Nature Methods*, vol. 17, pp. 261–272, 2020.

[29] W. McKinney, "pandas: a foundational python library for data analysis and statistics," *Python for High Performance and Scientific Computing*, vol. 14, 2011.

[30] J. D. Hunter, "Matplotlib: A 2d graphics environment," *Computing in Science & Engineering*, vol. 9, no. 3, pp. 90–95, 2007.